Published in final edited form as:
Curr Biol. 2012 May 8; 22(9): 753–762. doi:10.1016/j.cub.2012.02.069.

EB1-recruited microtubule +TIP complexes coordinate protrusion dynamics during 3D epithelial remodeling

Sarah Gierke and **Torsten Wittmann**[†]
Department of Cell and Tissue Biology, University of California, San Francisco, CA 94143

SUMMARY

Background—Epithelial remodeling, in which apical-basal polarized cells switch to a migratory phenotype, plays a central role in development and disease of multicellular organisms. Although dynamic microtubules (MTs) are required for directed migration on flat surfaces, how MT dynamics are controlled or contribute to epithelial remodeling in a more physiological three-dimensional (3D) environment is not understood. We use confocal live cell imaging to analyze MT function and dynamics during 3D epithelial morphogenesis and remodeling of polarized Madin-Darby canine kidney (MDCK) epithelial cells that undergo partial epithelial-to-mesenchymal transition (EMT) in response to hepatocyte growth factor (HGF).

Results—We find that HGF treatment increases MT growth rate before morphological changes are evident, and that large numbers of MTs grow into HGF-induced cell extensions independent of centrosome reorientation. Using lentivirus-mediated shRNA, we demonstrate that EB1, an adaptor protein that mediates recruitment of numerous other +TIP proteins to growing MT plus ends, is required for this HGF-induced MT reorganization. We further show that protrusion and adhesion dynamics are disorganized, and that vesicular trafficking to the tip of HGF-induced cell extensions is disrupted in EB1-depleted cells.

Conclusions—We conclude that EB1-mediated interactions with growing MTs are important to coordinate cell shape changes and directed migration into the surrounding extracellular matrix during epithelial remodeling in a physiological 3D environment. In contrast, EB1 is not required for the establishment or maintenance of apical-basal cell polarity, suggesting different functions of +TIPs and MTs in different types of cell polarity.

INTRODUCTION

Epithelial cells are typically polarized with a basal surface connecting to the underlying extracellular matrix (ECM), and an apical domain facing the topological outside of the organism. Although apical-basal polarity is critical to normal epithelial function and homeostasis, epithelial tissue architecture is remodeled during many developmental processes [1]. For example, branching morphogenesis during mammary gland or kidney tubule development requires that individual cells lose apical-basal polarity, change shape and acquire a more mesenchymal, migratory phenotype [2]. Such migratory cell shape changes are ultimately driven by reorganization of the cytoskeleton, a process that has been studied predominantly in cells migrating on flat and rigid 2D surfaces. In 2D, directed cell

[†]Corresponding author: torsten.wittmann@ucsf.edu, tel: +1 415 476 2603.

migration is primarily motored by actin polymerization that is required for leading edge protrusion. Adhesion turnover and myosin-mediated contractility further facilitate net forward movement. In many cell types, dynamic MTs are required to establish and maintain 2D directed migration. MT dynamics are spatiotemporally controlled with most growing MT ends facing toward the direction of migration [3,4]. However, to what extent MT dynamics are regulated or MTs contribute to cell shape changes in more physiologically relevant 3D environments is not known largely because of the technical challenges associated with high resolution microscopy of live cells embedded in a 3D matrix.

MTs are highly dynamic polymers that stochastically switch between phases of growth and shortening, and complex relationships exist between the regulation of MT growth dynamics and extracellular matrix properties in a 3D environment [5]. +TIPs, a heterogeneous group of proteins that reversibly bind to growing MT ends, have been proposed to control MT dynamics and interactions with other intracellular structures [6]. Specifically, the Adenomatous Polyposis Coli protein (APC), spectraplakins (ACF7), and CLASPs mediate MT interactions with cortical structures and signaling factors at the leading edge of migrating cells [7–9], and may be important regulators of cell architecture. Most +TIPs do not directly bind to growing MT ends, but are recruited by end-binding proteins (EBs) that have emerged as central components of +TIP protein interaction networks. EBs are small dimeric proteins consisting of an N-terminal calponin homology domain that directly recognizes a structural feature of growing MT ends, and a C-terminal EB homology domain that mediates localization of other +TIPs [10].

Here, we use a physiological 3D epithelial tissue culture system to address MT dynamics and function during epithelial morphogenesis and remodeling. ECM-embedded Madin-Darby canine kidney (MDCK) cells develop into spherical cysts with a central lumen and distinct apical-basal polarity. Stimulation with hepatocyte growth factor (HGF) results in 3D epithelial remodeling in which cells undergo a partial epithelial-to-mesenchymal transition (EMT) and send out dynamic cell extensions into the surrounding extracellular matrix [1,11]. Using spinning disk confocal microscopy we resolved the challenge of imaging real-time cytoskeleton behavior in 3D at high spatial and temporal resolution. We examine MT dynamics in both polarized MDCK cells and during epithelial remodeling by computational tracking, and we report extensive reorganization of the MT cytoskeleton and MT dynamics during HGF-induced cell shape changes. We further demonstrate that EB1 and +TIPs recruited to growing MT ends by EB1 are critically important for coordinated protrusion and cell-matrix adhesion dynamics during the early stages of HGF-induced epithelial remodeling.

RESULTS

Microtubule reorganization during epithelial remodeling in a 3D environment

In order to analyze MT function and dynamics during epithelial remodeling in a physiological 3D environment, we adapted an organogenesis model system for high-resolution spinning-disk confocal microscopy. Briefly, single MDCK cells seeded on coverslips coated with a thin Matrigel basement membrane matrix layer were overlaid with diluted Matrigel to allow development of polarized epithelial cysts. To induce partial EMT, cell outgrowth, and migration into the surrounding matrix, polarized cysts were treated with HGF after replacing the Matrigel overlay with collagen (Fig. 1B) [12,13].

We first compared polarized and HGF-treated cysts by immunofluorescence to determine how the cytoskeleton is reorganized during this morphological change. As expected, prior to HGF treatment, filamentous actin (F-actin) predominantly localized to cell-cell junctions and microvilli at the apical surface (Fig. 1A). The spherical geometry of MDCK cysts

allowed direct observation of apical, basal, and lateral MT arrays in different optical sections. MTs formed a dense network just below the apical microvilli and a less dense network at the basal surface. Cross-sections of perinuclear MT and F-actin bundles above the basal surface were consistent with MT organization typical for polarized epithelial cells [14], and MTs in medial sections were resolved much more clearly compared with z-axis reconstructions (Fig. 1A, bottom panel). HGF treatment resulted in extensive cytoskeleton reorganization. After 24 hours, individual cells had formed long extensions from the basal surface into the surrounding collagen matrix that often terminated in lamellipodia-like, F-actin-rich ruffles (Fig. 1C). In contrast to the relatively sparse basal MT network in polarized cysts, HGF-induced cell extensions contained numerous bundled MTs that extended into the distal extension tips (Fig. 1C, inset). MT acetylation was increased in HGF-induced extensions indicating increased MT stability compared with apical-basal polarized cells in which acetylated MTs were mostly localized to the apical surface and primary cilia (Fig. S1A) [15].

To test whether HGF-induced MT reorganization was mediated by centrosome reorientation toward the cell front as occurs in many cell types migrating on a 2D surface [4], we analyzed centrosome dynamics in HGF-induced extensions. In contrast to polarized cells in which both EGFP-γ-tubulin-marked centrosomes remained in close proximity near the apical surface, the two centrosomes often moved significantly apart in HGF-induced cell extensions (Fig. 1D,E). Typically, one centrosome remained close to the apical surface while the other one appeared to be pulled away, suggesting the presence of intracellular forces that may be unique to cell shape changes in a 3D environment. Nevertheless, both centrosomes remained behind the nucleus in the apical domain in >98% of cells with HGF-induced extensions ($n = 50$). Although centrosome reorientation may occur after cells lose their apical surface [16], it is not required for HGF-induced MT reorganization.

To directly visualize MT reorganization and dynamics in 3D epithelial structures, we expressed EB1 tagged with two EGFP moieties, EB1-2xEGFP, that yielded consistently bright signals on growing MT ends after optimization of imaging conditions (Fig. S1B,C). In both polarized and HGF-treated cells, the density of growing MT ends was highest in the apical domain, consistent with apical MT nucleation (Fig. 1F). Kymograph analysis indicated predominant MT growth toward the basal surface. In HGF-treated cysts, MTs continued to grow into cell extensions with increased growth rate and persistency. Growing MT ends also frequently bumped into and deformed the HGF-induced extension tip suggesting that MTs may mechanically contribute to protrusion or extension stability (Movie 1). Together these results suggest that MT reorganization during HGF-induced extension formation is mediated through regulation of MT growth dynamics.

EB1 is required for HGF-induced epithelial remodeling in 3D

EB1 is a central adaptor protein linking most +TIPs to growing MT ends, and EB1-recruited +TIP complexes likely play important roles in MT plus end dynamics and interactions [6,10]. To determine +TIP function during epithelial morphogenesis and remodeling, we targeted EB1 in MDCK cells by RNA interference. Because the canine genome contains predicted EB1 genes on over ten different chromosome loci, we developed eight short-hairpin RNA (shRNA) lentivirus constructs to target different combinations of homologous sequences. shRNA constructs #1 and #3 resulted in >95% depletion of EB1 protein (Fig. 2A). Although redundancy between EB1 and EB3 has been reported in other mammalian cell types [17], plus-end-tracking of three different EGFP-tagged +TIP proteins, CLASP2 [8,18], MCAK [10,19], and APC [10,20] was reduced ~5-fold in EB1-depleted cells (Fig. 2B; Fig. S2A), indicating that EB1 shRNA is an efficient tool to disrupt +TIP protein complexes at growing MT ends in MDCK cells.

We next tested how EB1 depletion affected epithelial cyst morphogenesis and HGF-induced remodeling. While most EB1-depleted cysts developed normally, there was a modest increase in the number of cysts with abnormally small or collapsed lumen (Fig. S2B,C,E). In addition, apical localization of podocalyxin (GP135) [21] indicated normal establishment of apical-basal polarity (Fig. S2D). In contrast, HGF-induced epithelial remodeling was markedly affected in EB1-depleted cells. After 16 hours in HGF, extensions formed by EB1-depleted cysts were significantly shorter, more branched, and appeared to retract and change direction more frequently than extensions and multicellular chains formed by control cysts (Fig. 2C,D; Movie 2). EB1 depletion also resulted in significant morphological differences in later stages of HGF-induced epithelial remodeling (Fig. S2F). Both shRNAs #1 and #3 produced identical defects in HGF-induced extension formation, indicating that the phenotype is EB1 specific (Fig. 2C,D). In addition, expression of a dominant negative EB1 fragment (EB1C, Fig. S1B) [17] similarly inhibited HGF-induced extension formation (Fig. S2G). Together these data indicate that EB1 plays an important role during epithelial remodeling in 3D.

EB1 is required for microtubule organization in HGF-induced cell extensions

To investigate the mechanism by which EB1 contributes to HGF-induced epithelial remodeling, we analyzed how EB1 depletion affected MT organization and dynamics in polarized and in HGF-treated cysts. Because MT growth is directed toward the basal surface (Fig. 1F) and EB1 is associated with basal MT arrays [22], we predicted that EB1 is required for MT interactions with the basal surface in polarized cells. Time-lapse microscopy of EGFP-α-tubulin confirmed that EB1-depleted cells had fewer, more curled MTs that displayed increased, rapid lateral movements consistent with a lack of cortical MT attachment (Fig. S3A; Movie 3) [8]. MT density was also decreased in EB1-depleted HGF-induced extensions, and MTs appeared laterally mobile (Fig. S3B, Movie 3). MT arrays did not reach the cell tip in contrast to straight, highly organized bundles in control cell extensions, further suggesting a defect in the stabilization of MT growth and organization toward the leading cell tip (Fig. S3C).

The high MT density and optical aberrations in the 3D system made it impossible to quantify MT dynamics using EGFP-α-tubulin. We therefore developed a double EGFP-tagged, shRNA#3-resistant, EB1 construct truncated at amino acid 248, EB1ΔC-2xEGFP (Fig. S1B). Although EB1ΔC-2xEGFP may rescue EB1-intrinsic effects on MT dynamics [17], it is not expected to restore EB1-dependent recruitment of other +TIPs to growing MT ends, and it did not rescue the EB1-depletion phenotype (Fig. 2E). We used computational tracking of EB1ΔC-2xEGFP to analyze MT dynamics [23,24]. Taking advantage of the spherical geometry of polarized MDCK cysts, we first compared apical, medial and basal optical sections (Fig. 3A,D; Fig S3D; Movie 4). In both control and EB1-depleted cysts, MTs in medial sections grew significantly faster than MTs in apical or basal sections. Analysis of MT growth rates as a function of track lifetime indicated that these differences are not an artifact of differing geometries of these MT networks (Fig. S3E,F). In contrast, differences between control and EB1-depleted cysts were small and mostly not statistically significant (Fig. 3D; Table S1).

MT growth dynamics were significantly changed in HGF-treated cells. MTs in the cell body and the bulk of HGF-induced extensions grew considerably faster than in polarized cells, although the growth rate decreased as MT ends approached the leading extension tip (Fig. 3B,E; Table S1; Movie 5). Strikingly, the MT growth rate was already significantly increased at the basal surface of HGF-treated cells prior to extension formation (Fig. 3F; Fig. S3G,H), indicating that HGF signaling directly stimulates MT growth, and that this increase is not solely due to cell shape changes. However, MT growth rates in HGF-induced extensions of EB1-depleted cells were indistinguishable from control cells, and a gradient in

growth rates between cell body and extension tip remained statistically significant (Fig. 3E). Nevertheless, MT growth tracks in EB1-depleted HGF-induced extensions were less organized and less directional than those of control extensions (Fig. 3B,C,G).

In addition, EB1-depleted HGF-induced cell extensions displayed a highly unusual MT behavior. EB1ΔC-2xEGFP-labeled MT ends often exhibited rapid and extensive retrograde movements (Fig. 3H; Movie 5). Because EB1 only associates with growing MT ends [6,24], these movements reflect retrograde translocations of growing MTs and are not due to MT depolymerization. Although some retrograde MT movements occurred in control HGF-induced extensions and average rates of these movements were similar in control (40 +/− 11 μm min^{-1}) and EB1-depleted cells (57 +/− 23 μm min^{-1}), they were much more frequent in EB1-depleted cells and covered significantly longer distances (Fig. 3I). Together these data demonstrate that during HGF-induced epithelial remodeling, EB1-recruited +TIP complexes do not appear to control spatial or HGF-induced differences in MT growth rates, but instead are required for proper reorganization and stabilization of the cell extension MT array.

EB1-depleted cells display uncoordinated protrusion and adhesion dynamics, and disrupted vesicle trafficking

To further characterize epithelial remodeling defects in EB1-depleted cells, we analyzed HGF-induced cell extension dynamics by imaging of mEGFP-Lifeact, a small yeast peptide that binds F-actin [25,26]. Control HGF-induced cells elongated persistently with a small F-actin-rich lamellipodia-like structure near the tip of the cell extension (Fig. 4A; Movie 6). In contrast, actin dynamics were increased and delocalized in EB1-depleted cells. Highly dynamic, short-lived Factin-rich ruffles formed along the length of the extension resulting in multiple branched protrusions and a lack of productive forward movement. These mislocalized actin dynamics were particularly evident in maximum intensity projections of mEGFP-Lifeact time-lapse sequences. Cells in control cysts mostly protruded directionally whereas EB1-depleted cysts had a fractal-like appearance indicative of extensive protrusion and retraction in many different directions (Fig. 4B).

The inability of EB1-depleted cells to stabilize a dominant protrusion indicated a failure to productively interact with the extracellular matrix. To investigate this we expressed paxillin-EGFP to visualize focal adhesion dynamics in HGF-induced cell extensions. Despite controversy over whether focal adhesions are relevant during cell migration in 3D [27], control cells formed pronounced focal adhesions at the distal end of the extension that appeared to mature and turn over in a coordinated manner as the extension tip advanced (Fig. 5A; Movie 7). This was severely disrupted in EB1-depleted extensions in which adhesions appeared uncoordinated with respect to protrusion advancement. Consequently, adhesions in EB1-depleted cells remained significantly less elongated, suggesting a defect in tension-mediated adhesion maturation (Fig. 5B).

We next analyzed HGF-treated cysts by high-resolution differential interference contrast (DIC) microscopy to test how such uncoordinated protrusion and adhesion dynamics affected cell-matrix interactions (Fig. 5C; Movie 8). Control extensions displayed long phases of persistent outgrowth that coincided with progressive pulling on and deformation of the collagen matrix. Pulling forces were evident by collagen fiber alignment in front of the extension as well as movement of fiduciary marks in the collagen matrix toward the extension tip (Fig. 5C, arrows). In contrast, EB1-depleted cells did not productively engage collagen fibers, resulting in little and non-directional net movement of the collagen matrix. To determine whether the apparent lack of focal adhesion maturation and absence of matrix pulling forces correlated with decreased actomyosin contractility, we stained HGF-treated cysts for myosin regulatory light chain phosphorylation (pMLC), the main activator of non-muscle myosin [28]. As reported previously, pMLC localized along cortical actin fibers in

control cell extensions (Fig. 5D) [16]. In contrast, in EB1-depleted cells we only observed punctate pMLC staining and no enrichment along the cortical actin cytoskeleton, indicating decreased actomyosin contractility (Fig. 5E).

Efficient vesicular trafficking is associated with directed migration [29–31] and depends on an intact MT cytoskeleton. To test whether disrupted trafficking could provide a mechanistic link between MT cytoskeleton defects and epithelial remodeling phenotypes in EB1-depleted cells, we analyzed the dynamics of VAMP3, a recycling endosome-associated SNARE that has been implicated in membrane, integrin and matrix metalloprotease transport to the leading edge [30,31]. In both control and EB1-depleted HGF-induced cells, EGFP-VAMP3 localized to the plasma membrane and to highly dynamic tubulovesicular structures that displayed rapid bidirectional movement along the length of cell extensions. In control cells, VAMP3-positive vesicles were closely associated with the tip of HGF-induced extensions and rapidly moved into newly formed membrane protrusions (Fig. 6A). In contrast, membrane protrusions that formed in EB1-depleted extensions often remained devoid of VAMP3-positive vesicular structures, likely because they lacked MT tracks. Although it was not possible to unambiguously detect or track individual vesicles, consistent with this observation, total EGFP-VAMP3 fluorescence was significantly enriched near the tip of HGF-induced extensions in control but not in EB1-depleted cells (Fig. 6B). Together these data suggest that EB1-mediated organization of the MT cytoskeleton and resulting directed vesicle delivery to the tip of HGF-induced extensions is required to coordinate cell-matrix adhesion and protrusion dynamics during 3D epithelial remodeling.

DISCUSSION

We report for the first time direct analysis and comparison of MT dynamics in apical-basal polarized epithelial cells and during growth factor induced epithelial remodeling by taking advantage of the spherical geometry of ECM-embedded apical-basal polarized epithelial cysts that allows optical sectioning in different planes. Adaptation of this tissue culture system such that epithelial structures are located within 30–50 μm of the coverslip surface allows spinning disk confocal microscopy with high N.A. oil immersion objectives. Although light scattering, spherical aberration, and lens-like properties of the epithelial sphere limit image resolution and signal intensity, equivalent high-resolution imaging of MT dynamics in epithelial cells in a 3D environment has not been achieved previously. We further used advanced computational tracking to quantify MT growth rates, thus gaining important insight into the mechanisms of MT reorganization during 3D epithelial remodeling. We believe these technical advances will be instrumental in future studies of intracellular movements of cytoskeletal components, organelles and other structures in a physiological 3D environment.

In polarized epithelial cells, MT minus ends are thought to be released from the centrosome and transported to tight junctions where they become anchored [32]. Consistent with MT minus end localization near the apical surface [14,32], we found that lateral MTs almost exclusively grew from the apical toward the basal cell surface. The growth rate of these lateral MTs was slightly but significantly increased compared with the more randomly organized apical and basal MT networks, demonstrating spatial MT regulation in polarized epithelial cells. Although MT growth at steep angles to the focal plane would result in apparently decreased growth rates, differences between different MT networks remained statistically significant for longer tracks that are more parallel to the section plane. Thus, random arrangement of MT growth directions likely increases the variance of growth rate populations, but still allows conclusions about relative differences between these populations. In HGF-induced cell extensions, the MT growth rate was increased further compared with apical-basal polarized cells. In addition, we observed spatial differences in

HGF-induced extensions in which the MT growth rate decreased significantly toward the extension tip similar to spatial gradients between the interior and lamella of epithelial cells in 2D cultures [8,24].

To analyze the function of +TIP proteins during MT organization in 3D epithelial structures, we targeted the central +TIP adaptor protein EB1 [10], and demonstrate that EB1 depletion in MDCK cells efficiently disrupts plus-end-tracking of different +TIPs. Both in polarized and HGF-stimulated cells, MT growth rates were largely independent of the +TIP binding activity of EB1, indicating that +TIP complexes do not function as global MT dynamics regulators. Because HGF stimulation results in sustained Pak1 activation downstream of Rac1 in MDCK cells [33], the HGF-induced growth rate increase could instead result from phosphorylation and inactivation of the MT destabilizer Op18/stathmin [34]. However, because we visualized growing MTs by expressing an EGFP-tagged EB1 MT-binding domain, we cannot exclude EB1-intrinsic effects on MT dynamics [17].

Nevertheless, EB1 depletion markedly disrupted MT organization in HGF-induced cell extensions. MTs often did not reach the cell extension tip, growing MT ends were less frequent and growth trajectories were disorganized. These MT organization defects are consistent with the proposed functions of a number of EB1-recruited +TIP proteins, including CLASPs, APC, and ACF7, which link MT plus ends to the cell cortex [7–9]. Defects in cortical MT interactions are also consistent with the frequent rapid and extensive retrograde movements of growing MT ends in EB1-depleted cells. Maximum rates of such retrograde MT translocations exceeded 100 μm min^{-1}, which is almost two orders of magnitude more rapid than typical actin retrograde flow in epithelial cells [35,36]. Thus, MT-actin coupling cannot explain these movements. Instead, we propose that they result from pulling forces on MTs in the cell body and sudden loss of +TIP-mediated MT interactions with the cell cortex. Although retrograde MT movements also occurred to a lesser extent in polarized EB1-depleted cysts (Movie 4), we rarely observed extensive retrograde MT translocations in cells plated on a 2D surface, indicating that the magnitude of these movements is related to unique forces acting on MTs in migrating cells in a 3D environment.

Finally, we show that EB1-mediated reorganization of the MT cytoskeleton is important for coordinated cell extension and adhesion dynamics during HGF-induced epithelial remodeling. Although the underlying molecular mechanism is likely complex and depends on multiple integrated functions of the MT cytoskeleton, +TIP-mediated stabilization of MTs in HGF-induced extensions is likely central to all these functions (Fig. 6C). MT dynamics have been proposed to directly influence Rho·GTPase signaling [4,37], which may be required for lamellipodia formation in a dominant extension tip and to restrict lateral protrusions. Mechanical resistance of stiff EB1-anchored MTs to contractile forces may be particularly important in a soft 3D environment to oppose cell retraction and contribute to extension elongation [38]. In addition, our data point toward a requirement of EB1-mediated stabilization of the MT cytoskeleton for efficient vesicular trafficking toward the tip of HGF-induced extensions. Reduced adhesion maturation and actomyosin contractility could be consistent with defects in integrin activation or recycling of adhesion components. Transport and recycling of integrins, and other adhesion or membrane components is likely more important during 3D cell shape remodeling and migration due to different geometrical constraints and potentially longer distances between the secretory machinery and the cell’s leading edge compared with cells on a 2D surface. Strikingly, although basal MT organization appeared disrupted in EB1-depleted polarized cells, EB1 depletion had very little effect on establishment or maintenance of apical-basal epithelial cell polarity. This may reflect incomplete EB1 knockdown or partial compensation by homologous proteins, however it does highlight different requirements for EB1 and consequently +TIP protein

functions in apical-basal polarity compared with front-back polarity of migrating cells. The similarity of MT organization in HGF-induced cell extensions to that in growing neurons [39] and fibroblasts migrating on linear tracks [40] further suggests a conserved role of +TIP complexes during cell migration in fibrillar 3D extracellular matrices. Thus, our work lays the foundation for future studies how cell shape changes are coordinated by intracellular signaling, cytoskeleton and adhesion dynamics in a physiological 3D environment.

EXPERIMENTAL PROCEDURES

MDCK cells were cultured as described [12]. Stable EB1-depleted cell lines were generated by pLKO.1 lentivirus-mediated shRNA [41,42]. Imaging was on a custom-built spinning disk confocal microscope [41]. MT growth rates were determined using plusTipTracker [23]. All other image analysis was performed in NIS Elements (Nikon). Detailed experimental procedures are included in the Supplemental Material.

Highlights

- High resolution microscopy of epithelial cell cytoskeleton dynamics in a 3D environment
- Microtubule dynamics are spatiotemporally regulated during 3D epithelial remodeling
- EB1 coordinates protrusion and adhesion dynamics during 3D epithelial remodeling
- EB1ΔC-2xEGFP is a novel tool to track microtubule growth with high signal-to-noise

Supplementary Material

Refer to Web version on PubMed Central for supplementary material.

Acknowledgments

We thank members of the Mostov lab, D. Bryant and C. Jacobson for initial help with MDCK cyst cultures, and D. Eastburn and D. Bryant for paxillin-EGFP and EGFP-VAMP3 expressing MDCK cells. We also thank R. Wedlich-Soldner for Lifeact, the Genentech Reagents Program for HGF, M. Bagonis and the Danuser lab for help with plusTipTracker, P. Kumar for help with cloning, D. Barber and the Wittmann and Barber labs for support, productive discussions and baked goods. This work was supported by a US National Sciences Foundation Graduate Research fellowship to S.G., and US National Institutes of Health grant R01 GM079139 to T.W. Research was conducted in a facility constructed with support from the Research Facilities Improvement Program grant C06 RR16490 and on instrumentation funded by Shared Equipment grant S10 RR026758 from the National Center for Research Resources of the National Institutes of Health.

REFERENCES

1. Bryant DM, Mostov KE. From cells to organs: building polarized tissue. Nat. Rev. Mol. Cell Biol. 2008; 9:887–901. [PubMed: 18946477]
2. Affolter M, Zeller R, Caussinus E. Tissue remodelling through branching morphogenesis. Nat. Rev. Mol. Cell Biol. 2009; 10:831–842. [PubMed: 19888266]
3. Kaverina I, Straube A. Regulation of cell migration by dynamic microtubules. Semin. Cell Dev. Biol. 2011; 22:968–974. [PubMed: 22001384]
4. Wittmann T, Waterman-Storer CM. Cell motility: can Rho GTPases and microtubules point the way? J. Cell Sci. 2001; 114:3795–3803. [PubMed: 11719546]

5. Myers KA, Applegate KT, Danuser G, Fischer RS, Waterman CM. Distinct ECM mechanosensing pathways regulate microtubule dynamics to control endothelial cell branching morphogenesis. J. Cell Biol. 2011; 192:321–334. [PubMed: 21263030]
6. Akhmanova A, Steinmetz MO. Tracking the ends: a dynamic protein network controls the fate of microtubule tips. Nat. Rev. Mol. Cell Biol. 2008; 9:309–322. [PubMed: 18322465]
7. Etienne-Manneville S. APC in cell migration. Adv. Exp. Med. Biol. 2009; 656:30–40. [PubMed: 19928350]
8. Kumar P, Lyle KS, Gierke S, Matov A, Danuser G, Wittmann T. GSK3beta phosphorylation modulates CLASP-microtubule association and lamella microtubule attachment. J. Cell Biol. 2009; 184:895–908. [PubMed: 19289791]
9. Wu X, Shen QT, Oristian DS, Lu CP, Zheng Q, Wang HW, Fuchs E. Skin stem cells orchestrate directional migration by regulating microtubule-ACF7 connections through GSK3beta. Cell. 2011; 144:341–352. [PubMed: 21295697]
10. Honnappa S, Gouveia SM, Weisbrich A, Damberger FF, Bhavesh NS, Jawhari H, Grigoriev I, van Rijssel FJ, Buey RM, Lawera A, et al. An EB1-binding motif acts as a microtubule tip localization signal. Cell. 2009; 138:366–376. [PubMed: 19632184]
11. Leroy P, Mostov KE. Slug is required for cell survival during partial epithelial-mesenchymal transition of HGF-induced tubulogenesis. Mol. Biol. Cell. 2007; 18:1943–1952. [PubMed: 17344479]
12. O'Brien LE, Yu W, Tang K, Jou TS, Zegers MM, Mostov KE. Morphological and biochemical analysis of Rac1 in three-dimensional epithelial cell cultures. Methods Enzymol. 2006; 406:676–691. [PubMed: 16472697]
13. Kwon SH, Nedvetsky PI, Mostov KE. Transcriptional profiling identifies TNS4 function in epithelial tubulogenesis. Curr. Biol. 2011; 21:161–166. [PubMed: 21236678]
14. Bacallao R, Antony C, Dotti C, Karsenti E, Stelzer EH, Simons K. The subcellular organization of Madin-Darby canine kidney cells during the formation of a polarized epithelium. J. Cell Biol. 1989; 109:2817–2832. [PubMed: 2592406]
15. Jaulin F, Kreitzer G. KIF17 stabilizes microtubules and contributes to epithelial morphogenesis by acting at MT plus ends with EB1 and APC. J. Cell Biol. 2010; 190:443–460. [PubMed: 20696710]
16. Yu W, O'Brien LE, Wang F, Bourne H, Mostov KE, Zegers MM. Hepatocyte growth factor switches orientation of polarity and mode of movement during morphogenesis of multicellular epithelial structures. Mol. Biol. Cell. 2003; 14:748–763. [PubMed: 12589067]
17. Komarova Y, De Groot CO, Grigoriev I, Gouveia SM, Munteanu EL, Schober JM, Honnappa S, Buey RM, Hoogenraad CC, Dogterom M, et al. Mammalian end binding proteins control persistent microtubule growth. J. Cell Biol. 2009; 184:691–706. [PubMed: 19255245]
18. Mimori-Kiyosue Y, Grigoriev I, Lansbergen G, Sasaki H, Matsui C, Severin F, Galjart N, Grosveld F, Vorobjev I, Tsukita S, et al. CLASP1 and CLASP2 bind to EB1 and regulate microtubule plus-end dynamics at the cell cortex. J. Cell Biol. 2005; 168:141–153. [PubMed: 15631994]
19. Moore AT, Rankin KE, von DG, Peris L, Wagenbach M, Ovechkina Y, Andrieux A, Job D, Wordeman L. MCAK associates with the tips of polymerizing microtubules. J. Cell Biol. 2005; 169:391–397. [PubMed: 15883193]
20. Slep KC, Rogers SL, Elliott SL, Ohkura H, Kolodziej PA, Vale RD. Structural determinants for EB1-mediated recruitment of APC and spectraplakins to the microtubule plus end. J. Cell Biol. 2005; 168:587–598. [PubMed: 15699215]
21. Ojakian GK, Schwimmer R. The polarized distribution of an apical cell surface glycoprotein is maintained by interactions with the cytoskeleton of Madin-Darby canine kidney cells. J. Cell Biol. 1988; 107:2377–2387. [PubMed: 3198692]
22. Reilein A, Nelson WJ. APC is a component of an organizing template for cortical microtubule networks. Nat. Cell Biol. 2005; 7:463–473. [PubMed: 15892196]
23. Applegate KT, Besson S, Matov A, Bagonis MH, Jaqaman K, Danuser G. plusTipTracker: Quantitative image analysis software for the measurement of microtubule dynamics. J. Struct. Biol. 2011; 176:168–184. [PubMed: 21821130]

24. Matov A, Applegate K, Kumar P, Thoma C, Krek W, Danuser G, Wittmann T. Analysis of microtubule dynamic instability using a plus-end growth marker. Nat. Methods. 2010; 7:761–768. [PubMed: 20729842]
25. Riedl J, Crevenna AH, Kessenbrock K, Yu JH, Neukirchen D, Bista M, Bradke F, Jenne D, Holak TA, Werb Z, et al. Lifeact: a versatile marker to visualize F-actin. Nat. Methods. 2008; 5:605–607. [PubMed: 18536722]
26. Haynes J, Srivastava J, Madson N, Wittmann T, Barber DL. Dynamic actin remodeling during epithelial-mesenchymal transition depends on increased moesin expression. Mol. Biol. Cell. 2011; 22:4750–4764. [PubMed: 22031288]
27. Harunaga JS, Yamada KM. Cell-matrix adhesions in 3D. Matrix Biol. 2011; 30:363–368. [PubMed: 21723391]
28. Vicente-Manzanares M, Ma X, Adelstein RS, Horwitz AR. Non-muscle myosin II takes centre stage in cell adhesion and migration. Nat. Rev. Mol. Cell Biol. 2009; 10:778–790. [PubMed: 19851336]
29. Prigozhina NL, Waterman-Storer CM. Decreased polarity and increased random motility in PtK1 epithelial cells correlate with inhibition of endosomal recycling. J. Cell Sci. 2006; 119:3571–3582. [PubMed: 16931597]
30. Veale KJ, Offenhauser C, Whittaker SP, Estrella RP, Murray RZ. Recycling endosome membrane incorporation into the leading edge regulates lamellipodia formation and macrophage migration. Traffic. 2010; 11:1370–1379. [PubMed: 20604897]
31. Kean MJ, Williams KC, Skalski M, Myers D, Burtnik A, Foster D, Coppolino MG. VAMP3, syntaxin-13 and SNAP23 are involved in secretion of matrix metalloproteinases, degradation of the extracellular matrix and cell invasion. J. Cell Sci. 2009; 122:4089–4098. [PubMed: 19910495]
32. Bellett G, Carter JM, Keynton J, Goldspink D, James C, Moss DK, Mogensen MM. Microtubule plus-end and minus-end capture at adherens junctions is involved in the assembly of apico-basal arrays in polarised epithelial cells. Cell Motil. Cytoskeleton. 2009; 66:893–908. [PubMed: 19479825]
33. Royal I, Lamarche-Vane N, Lamorte L, Kaibuchi K, Park M. Activation of cdc42, rac, PAK, and rho-kinase in response to hepatocyte growth factor differentially regulates epithelial cell colony spreading and dissociation. Mol. Biol. Cell. 2000; 11:1709–1725. [PubMed: 10793146]
34. Wittmann T, Bokoch GM, Waterman-Storer CM. Regulation of microtubule destabilizing activity of Op18/stathmin downstream of Rac1. J. Biol. Chem. 2004; 279:6196–6203. [PubMed: 14645234]
35. Waterman-Storer CM, Salmon ED. Actomyosin-based retrograde flow of microtubules in the lamella of migrating epithelial cells influences microtubule dynamic instability and turnover and is associated with microtubule breakage and treadmilling. J. Cell Biol. 1997; 139:417–434. [PubMed: 9334345]
36. Wittmann T, Bokoch GM, Waterman-Storer CM. Regulation of leading edge microtubule and actin dynamics downstream of Rac1. J. Cell Biol. 2003; 161:845–851. [PubMed: 12796474]
37. Birkenfeld J, Nalbant P, Yoon SH, Bokoch GM. Cellular functions of GEF-H1, a microtubule-regulated Rho-GEF: is altered GEF-H1 activity a crucial determinant of disease pathogenesis? Trends Cell Biol. 2008; 18:210–219. [PubMed: 18394899]
38. Wang N, Naruse K, Stamenovic D, Fredberg JJ, Mijailovich SM, Tolic-Norrelykke IM, Polte T, Mannix R, Ingber DE. Mechanical behavior in living cells consistent with the tensegrity model. Proc. Natl. Acad. Sci. U. S. A. 2001; 98:7765–7770. [PubMed: 11438729]
39. Conde C, Caceres A. Microtubule assembly, organization and dynamics in axons and dendrites. Nat. Rev. Neurosci. 2009; 10:319–332. [PubMed: 19377501]
40. Doyle AD, Wang FW, Matsumoto K, Yamada KM. One-dimensional topography underlies three-dimensional fibrillar cell migration. J. Cell Biol. 2009; 184:481–490. [PubMed: 19221195]
41. Stehbens S, Pemble H, Murrow L, Wittmann T. Imaging intracellular protein dynamics by spinning disk confocal microscopy. Methods Enzymol. 2012; 504:293–313. [PubMed: 22264541]
42. Moffat J, Grueneberg DA, Yang X, Kim SY, Kloepfer AM, Hinkle G, Piqani B, Eisenhaure TM, Luo B, Grenier JK, et al. A lentiviral RNAi library for human and mouse genes applied to an arrayed viral high-content screen. Cell. 2006; 124:1283–1298. [PubMed: 16564017]

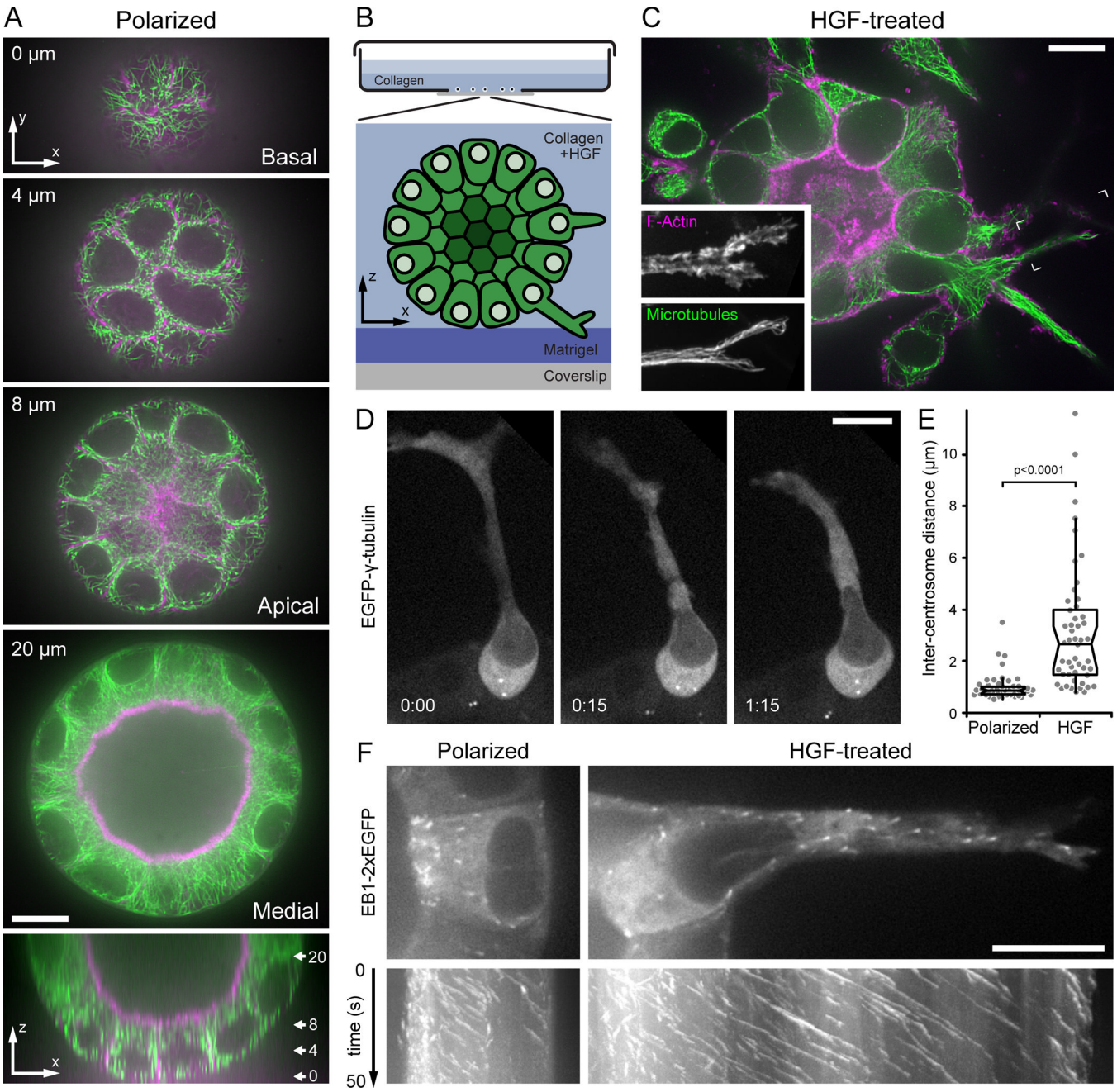

Figure 1. Microtubule cytoskeleton reorganization during HGF-induced epithelial remodeling

(A) Spinning disk confocal microscopy optical sections of a polarized MDCK cyst stained for F-actin (magenta) and MTs (green). Distance from the bottom of the cyst is indicated. The bottom panel is a z-axis reconstruction, and the approximate location of the optical sections shown is indicated. (B) Diagram of the 3D MDCK epithelial culture system adapted for high-resolution imaging. (C) Single optical section of F-actin (magenta) and MTs (green) 24 hours after HGF addition. Insets show a maximum intensity projection of the indicated area at higher magnification to illustrate the dense MT array extending to the extension tip. (D) EGFP-γ-tubulin time-lapse sequence in an HGF-induced extension showing centrosome separation and dynamics. Centrosomes remain close in the neighboring polarized cell that has not formed an extension. Elapsed time is indicated in hours:minutes. (E) Distance

between centrosomes in untreated polarized cells and cells with HGF-induced extensions. Gray symbols are measurements from individual cells ($n = 50$). (F) Images from medial optical sections of EB1-2xEGFP time-lapse sequences recorded at 2 frames s^{-1} with the apical surface oriented to the left. The bottom panels show kymographs perpendicular to the apical-basal cell axis. Oblique lines represent MT ends growing toward the basal surface or into the HGF-induced extension, respectively. Scale bars, 10 μm. See also Fig. S1 and Movie 1.

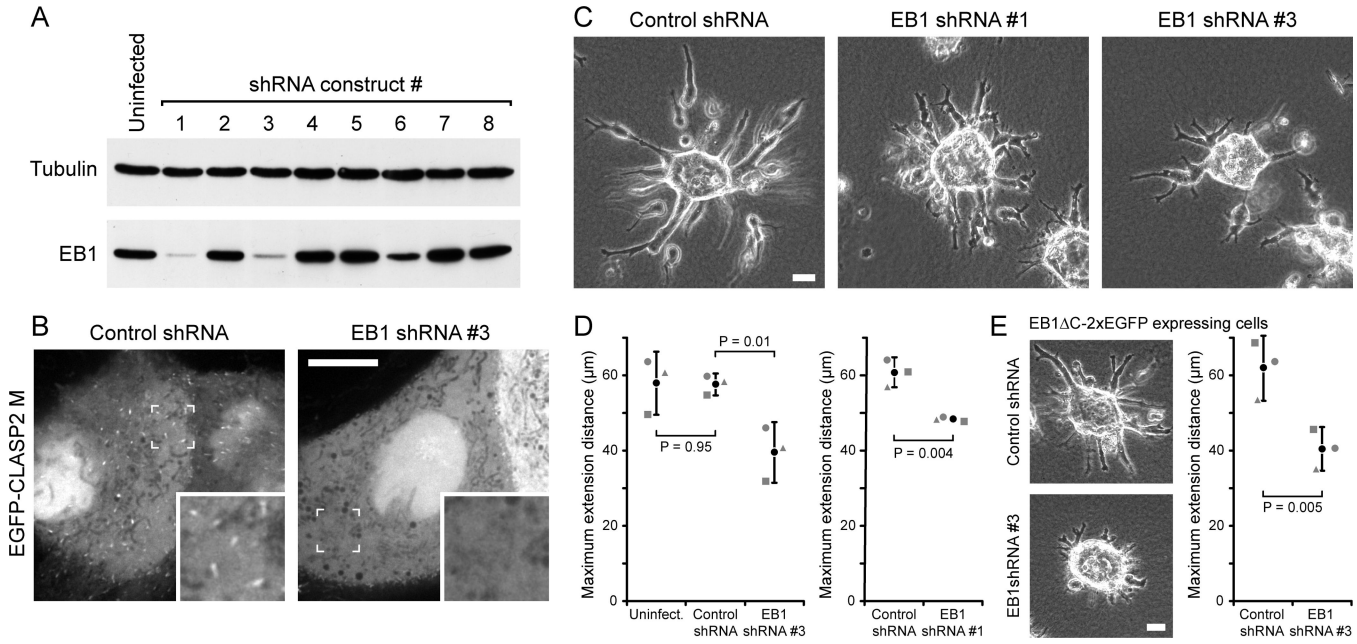

Figure 2. EB1 is required for HGF-induced epithelial remodeling

(A) Immunoblot of lysates from cells expressing different shRNA constructs after 7 days of puromycin selection. Tubulin was used as loading control. (B) MDCK cells stably expressing control or EB1 shRNA#3, transiently transfected with an EGFP-tagged, non-phosphorylatable construct encoding the CLASP2 EB1-binding domain (CLASP2 M) [8]. Insets show indicated region at higher magnification. Scale bar, 10 μm. (C) Phase contrast images of control and EB1-depleted HGF-treated MDCK cysts. Scale bar, 20 μm. (D) Quantification of HGF-induced cell extension into the surrounding collagen matrix. Graphs shows the average length of the three longest extensions measured from extension tip to cyst edge. Gray symbols are the average of 80–100 cysts from 3 separate experiments. Black circle represents the average of these three experiments. Error bars indicate 95% confidence interval. (E) Phase contrast images of EB1ΔC-2xEGFP-expressing control and EB1-depleted HGF-treated MDCK cysts, and quantification of HGF-induced cell extensions as in (D). Scale bar, 20 μm. See also Fig. S2 and Movie 2.

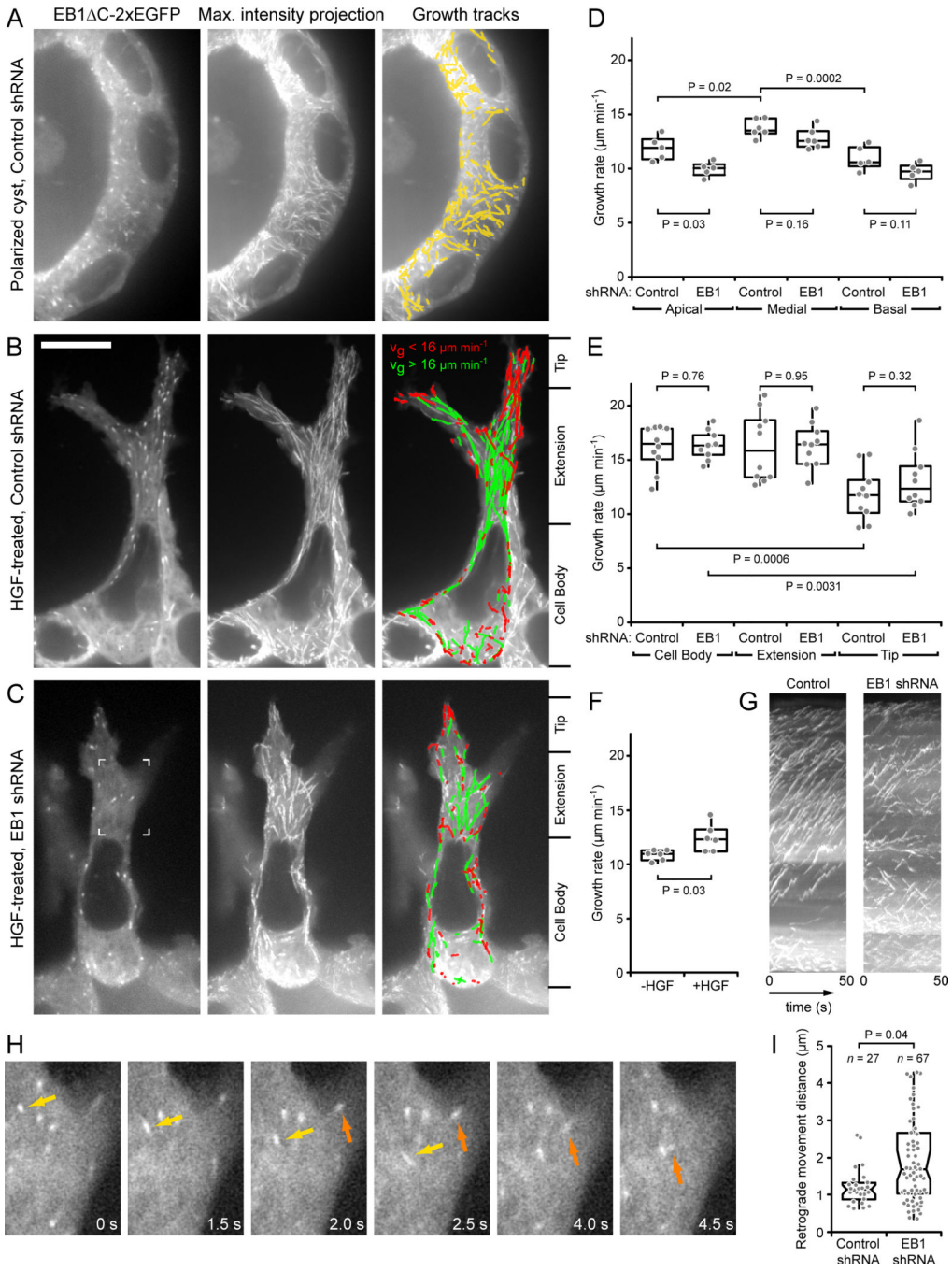

Figure 3. Analysis of microtubule dynamics in 3D epithelial structures

(A–C) Representative images of EB1ΔC-2xEGFP tracking in (A) a polarized, control shRNA cyst, and HGF-induced extensions of (B) control and (C) EB1-depleted cysts. Left panels are single images of the time-lapse sequence, middle panels show maximum intensity projections over the entire sequence (100 frames recorded at 2 frames s^{-1}), and right panels show computer-generated tracks overlaid on the maximum intensity projection indicating tracking quality. Only tracks with a lifetime of >2.5 s are shown. Tracks in (B) and (C) are color-coded for growth rate. (D) MT growth rates in apical, medial, and basal optical sections in control or EB1-depleted polarized cysts. (E) MT growth rates in the cell body, extension and extension tip in control or EB1-depleted HGF-induced extensions. Division of

cells into these three regions is indicated on the right of (B) and (C). (F) MT growth rates in basal optical sections in polarized cysts in Matrigel expressing EB1-2xEGFP before and 5 hrs after HGF addition. (D–F) Gray symbols represent the average growth rate of all tracks per cell and indicated condition. P-values of relevant comparisons are indicated on the graphs. (G) Kymographs of the cells shown in (B) and (C). (H) EB1ΔC-2xEGFP time-lapse sequence in an EB1-depleted HGF-induced extension. The region shown is indicated in (C). Two growing MT ends that display extensive retrograde movements are highlighted by arrows. Elapsed time is in seconds. (I) Number and distance of all retrograde MT movements in ten control and EB1-depleted HGF-induced extensions. Each gray symbol represents a retrograde movement event. Scale bar, 10 μm. See also Fig. S3, Movies 3, 4 and 5.

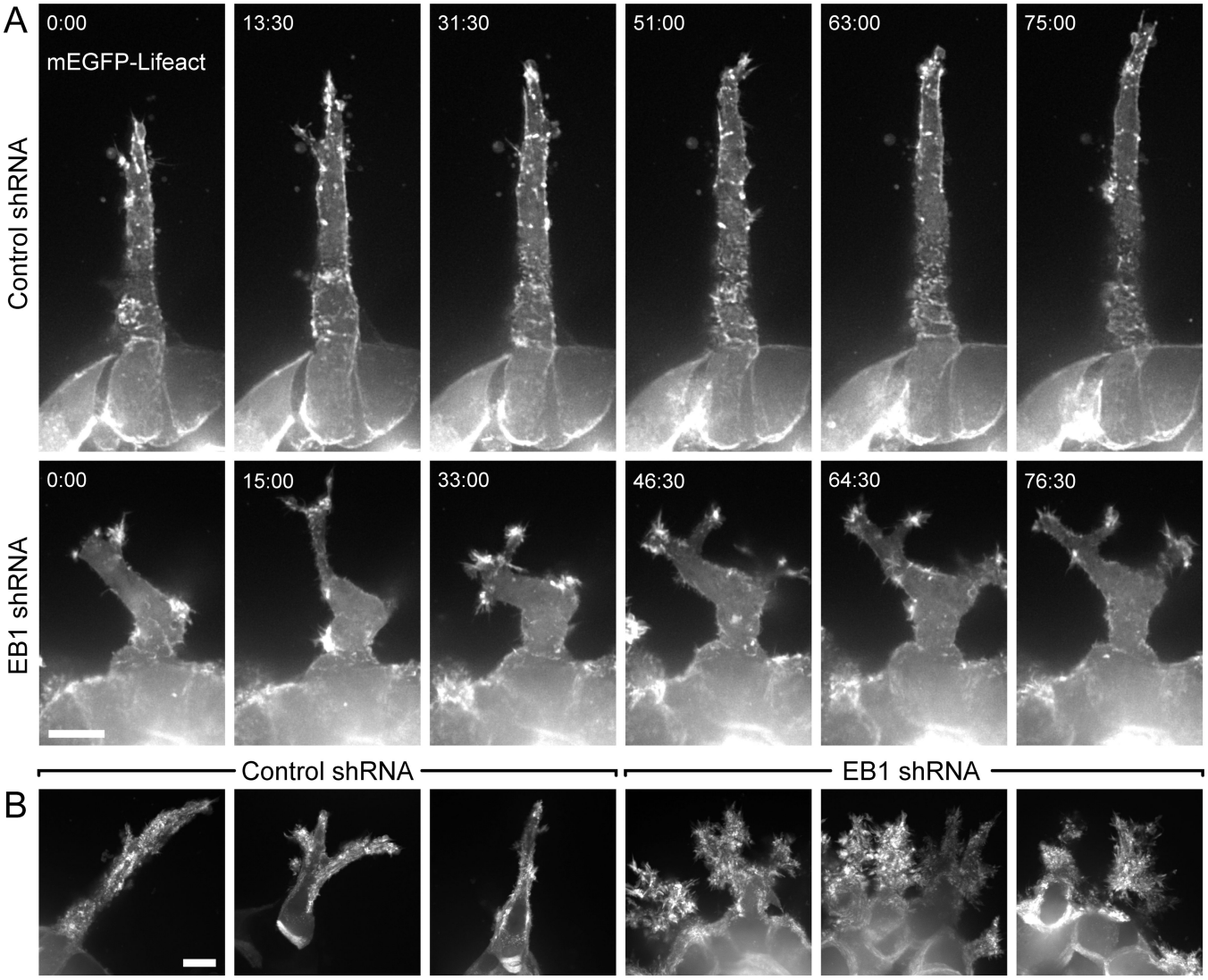

Figure 4. Uncoordinated protrusion dynamics in EB1-depleted cells

(A) mEGFP-Lifeact time-lapse sequences of HGF-induced extensions in control and EB1-depleted cysts. Each image is a maximum intensity projection of three optical sections (2 μm between sections) to compensate for cell movement out of the plane of focus. Elapsed time is in minutes:seconds. (B) Maximum intensity projection over two hour time-lapse sequences, which highlights increased and uncoordinated actin dynamics in EB1-depleted cells. Scale bars, 10 μm. See also Movie 6.

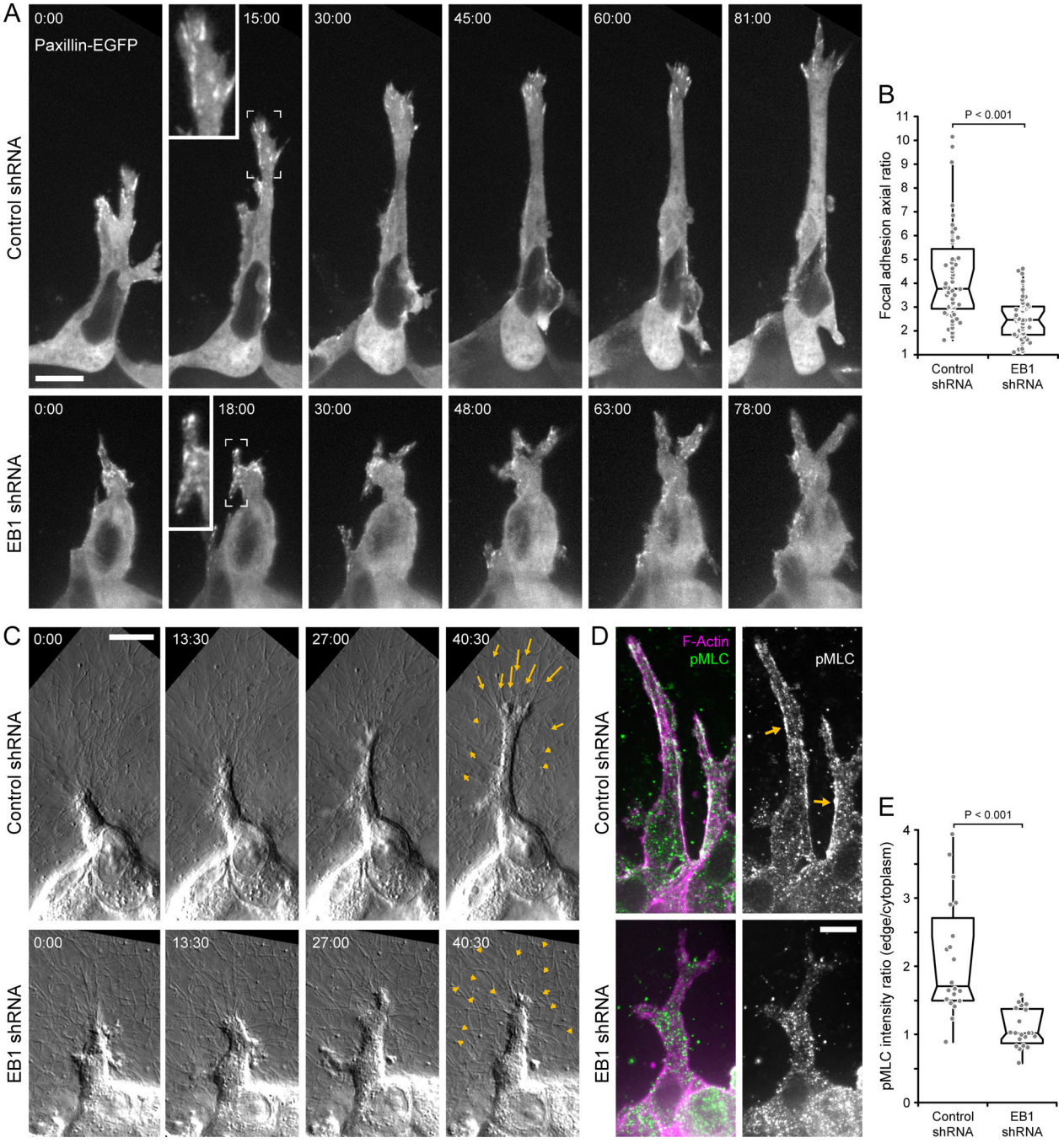

Figure 5. EB1 is required for productive interactions with the extracellular matrix

(A) Paxillin-EGFP time-lapse sequences of HGF-induced extensions in control and EB1-depleted cysts. Each image is a maximum intensity projection of three optical sections (1 μm between sections). Insets show higher magnification of indicated areas. (B) Axial ratio, defined as long divided by short axis, of focal adhesions in control and EB1-depleted extensions. The three longest adhesions were measured for each extension and each circle represents one adhesion (n = 60 adhesions in 20 cells). (C) DIC time-lapse sequences of HGF-induced extensions protruding into the surrounding fibrillar collagen matrix. Arrows indicate movement of fiduciary marks in the collagen between first and last frame shown. Elapsed time is indicated in minutes:seconds in (A) and (C). (D) pMLC

immunofluorescence in HGF-induced extensions. Each image is a maximum intensity projection of three optical sections (1 μm between sections). Arrows indicate pMLC staining along cortical actin cables in control cells. (E) Ratio of pMLC fluorescence intensity along cell extension edge and cytoplasm. (n = 20 cell extensions). See also Movies 7 and 8. Scale bars, 10 μm.

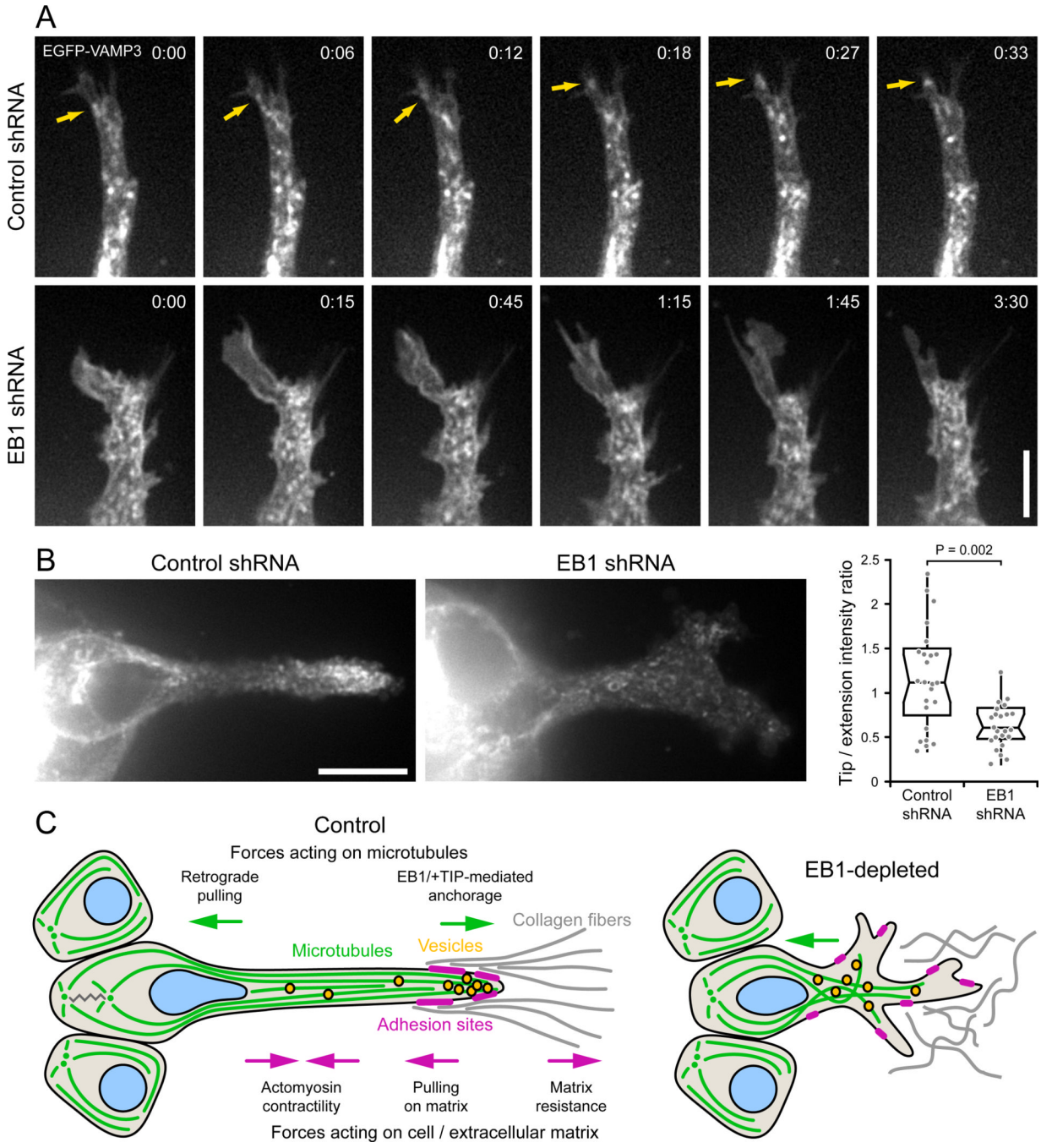

Figure 6. EB1 depletion disrupts VAMP3-positive vesicle trafficking to the extension tip

(A) EGFP-VAMP3 time-lapse sequences of control and EB1-depleted HGF-induced extensions. Faster time scale in control cell demonstrates the rapid movement of vesicles into the extension tip, while the membrane protrusion in the EB1-depleted cell remains vacant over a much longer time period. Arrows indicate vesicle movement into the extension tip. Elapsed time is indicated in minutes:seconds. Scale bar, 5 μm. (B) VAMP3-positive vesicles accumulate near the extension tip in control cells. The graph shows a quantification of the ratio of EGFP-VAMP3 fluorescence intensity near the extension tip and in the middle of the cell extension (n = 25 cells). Scale bar, 10 μm. (C) Model of EB1 contribution to cell migration in a 3D environment. EB1-recruited +TIP complexes anchor

and stabilize MTs along the HGF-induced cell extension, providing mechanical resistance to contractile forces in the cell body and establishing transport tracks toward the extension tip.